



AMERICAN METEOROLOGICAL SOCIETY

Journal of Applied Meteorology and Climatology

EARLY ONLINE RELEASE

This is a preliminary PDF of the author-produced manuscript that has been peer-reviewed and accepted for publication. Since it is being posted so soon after acceptance, it has not yet been copyedited, formatted, or processed by AMS Publications. This preliminary version of the manuscript may be downloaded, distributed, and cited, but please be aware that there will be visual differences and possibly some content differences between this version and the final published version.

The DOI for this manuscript is doi: 10.1175/2008JAMC1876.1

The final published version of this manuscript will replace the preliminary version at the above DOI once it is available.



Diagnosing the Intercept Parameter for Exponential Raindrop Size Distribution Based on Video Disdrometer Observations: Model Development

Guifu Zhang¹, Ming Xue^{1,2}, Qing Cao¹ and Daniel Dawson^{1,2}

¹School of Meteorology and ²Center for Analysis and Prediction of Storms
University of Oklahoma

Submitted to J. Applied Meteorology and Climatology

Initial submission September 2007

Revised February, 2008

Corresponding author address:

Dr. Guifu Zhang

School of Meteorology

University of Oklahoma

120 David L. Boren Blvd, Suite 5900

Norman, OK 73072, USA

E-mail: guzhang1@ou.edu

Abstract

The exponential distribution $N(D) = N_0 \exp(-\Lambda D)$ with a fixed intercept parameter N_0 is most commonly used to represent raindrop size distribution (DSD) in rainfall estimation and in single-moment bulk microphysics parameterization schemes. Disdrometer observations show that the intercept parameter is far from constant and systematically depends on the rain type and intensity. In this study, a diagnostic relation of N_0 as a function of rain water content (W) is derived based on Two-Dimensional Video Disdrometer (2DVD) measurements. The data reveal a clear correlation between N_0 and the rain water content (W) where N_0 increases as W increases. To minimize the effects of sampling error, a relation between two middle moments is used to derive the $N_0 - W$ relation. This diagnostic relation has the potential to improve rainfall estimation and bulk microphysics parameterizations. A parameterization scheme for warm rain processes based on the diagnostic N_0 DSD model is formulated and presented. The diagnostic N_0 -based parameterization scheme yields less evaporation and accretion for stratiform rain than that using fixed- N_0 .

1. Introduction

Information about the drop size distribution (DSD) is essential for understanding precipitation physics, estimating rainfall, and improving microphysics parameterizations in numerical weather prediction (NWP) models (Steiner et al. 2004). The characteristics of rain DSDs are often associated with the types of storms (e.g., convective versus stratiform rain) and their stages of development (e.g., the developing versus decaying stage, Brandes et al. 2006). Strong convective rain usually contains both large and small drops and has a broad DSD while the decaying stage of a convection is often dominated by small drops. Stratiform rain usually contains relatively larger drops but has a low number concentration for a given rain rate (Zhang et al. 2006).

Rain DSDs are usually represented by distribution models, such as the exponential distribution, Gamma distribution, and lognormal distribution models. A DSD model usually contains a few free parameters that should be easy to determine and the model should be capable of capturing the main physical processes and properties. The exponential distribution with two free parameters is the most commonly used DSD model that has some of these properties, and it is given by

$$N(D) = N_0 \exp(-\Lambda D), \quad (1)$$

where N_0 ($\text{m}^{-3} \text{mm}^{-1}$) is the intercept parameter and Λ (mm^{-1}) is a slope parameter. A single-moment bulk microphysics model predicts one of the moments of the DSD, which determines one of the two parameters. Either the intercept parameter N_0 or the slope Λ is fixed so that the other parameter Λ (or N_0) is uniquely related to the predicted water content, W (g m^{-3}), which in turn is linearly related to the 3rd moment of the DSD. The Marshall–Palmer (M-P, Marshall and Palmer 1948) exponential DSD model with the N_0 value fixed at $8000 \text{ m}^{-3} \text{mm}^{-1} = 8 \times 10^6 \text{ m}^{-4}$ is widely used for representing warm rain (Kessler 1969) and ice (e.g., Lin et al. 1983; Hong et al. 2004)

microphysics. In a microphysics scheme used by the RAMS model, the slope parameter Λ is fixed and the N_0 is determined from the W (Walko et al. 1995). The single-moment schemes are computationally efficient and widely used in research and operational NWP models.

In NWP model simulations, forecast results are sensitive to the DSD parameters chosen (e.g., Gilmore et al. 2004; van den Heever and Cotton 2004; Tong and Xue 2008). While one of the exponential distribution parameters needs to be fixed in single-moment schemes, two-moment schemes allow more flexibility in representing DSDs by determining both parameters from two prognostic state variables (often the mixing ratio and total number concentration). The Gamma distribution has also been used in two- and three-moment parameterization schemes (Meyers et al. 1997; Milbrandt and Yao 2005a,b; Seifert 2005), allowing for varying shape parameters of DSDs. While the exponential distribution may be sufficient for snowflakes, the Gamma distribution has the advantage of better characterizing hail size distributions where there are few small particles.

Recent disdrometer observations have indicated that the N_0 and number concentration (N_t) are not constant, but vary depending on precipitation type, rain intensity and stage of development. Waldvogel (1974) found large changes in N_0 for DSDs at different heights in profiling radar data. Sauvageot and Lacaux (1995) showed variations of both N_0 and Λ from impact disdrometer measurements. Recent observations by 2D Video Disdrometers (2DVD) suggest that rain DSDs are better represented by a constrained Gamma distribution (Zhang et al. 2001) that also contains two free parameters. In Zhang et al. (2006), the constrained Gamma model was further simplified to a single parameter model for bulk microphysical parameterization, which produced more accurate precipitation system forecasts than the M-P model. Since the exponential distribution model is widely used, a diagnostic relation of N_0 as a function of W would improve rain estimation and microphysical parameterizations that are based on such an improved model. Thompson et al.

(2004) proposed a diagnostic N_0 relation using a hyperbolic tangent function to represent drizzle-type rain for winter weather prediction, which has not been verified by observations. The relation yields too many small drops and hence too much evaporation, which may not be applicable to summer time convection or stratiform rain types.

In this study, we derive a diagnostic N_0 relation from rain DSD data that were collected in Oklahoma using disdrometers. To minimize the error effects introduced in the fitting procedure, we formulate the problem with a relation between two DSD moments. A diagnostic relation is found from the relation between two middle moments. Section 2 describes methods of deriving the diagnostic relation and section 3 presents results of diagnosing N_0 from water content using 2DVD measurements. In Section 4, we discuss applications of the diagnostic relation in the parameterization of rain physics and microphysical processes. Final summary and discussions are given in section 5.

2. Diagnosing methods

The diagnostic relation for the intercept parameter N_0 as a function of water content can be derived using two different approaches: (i) the direct fitting approach (DFA) and (ii) the moment relation method (MRM), described as follows.

The DFA is to first find the DSD parameters (N_0, Λ) by fitting DSD (e.g., disdrometer) data to the exponential function (1) for each DSD, and then plot the estimated N_0 versus W for the whole dataset to obtain a mean relation.

The n^{th} moment of the exponential DSD (1) is

$$M_n = \int D^n N(D) dD = N_0 \Lambda^{-(n+1)} \Gamma(n+1) \quad . \quad (2)$$

Hence, the DSD parameters, N_0 and Λ , can be determined from any two moments (M_l, M_m) as

$$\Lambda = \left(\frac{M_l \Gamma(m+1)}{M_m \Gamma(l+1)} \right)^{\frac{1}{m-l}}, \quad (3)$$

$$N_0 = \frac{M_l \Lambda^{l+1}}{\Gamma(l+1)}. \quad (4)$$

When N_0 is obtained along with the water content W for DSD data sets, a $N_0 - W$ relation can be found through another fitting procedure, e.g., power-law fitting. It is noted that the values of the estimated N_0 depend on which two moments are used and on the accuracy of the two moment estimates. Since the estimates of both the moments (M_l, M_m) have error, the DSD parameters (N_0, Λ) obtained from them will also have error. The natural variation in DSDs and model error also causes a large scatter in the $N_0 - W$ plot (see Fig. 2 in next section). The estimation error and natural variation are very difficult to separate unless two or more instruments are used (Cao et al. 2008). Hence, the $N_0 - W$ relation derived from the above procedure tends to have larger errors than those produced by the MRM procedure discussed below.

To minimize the error effects introduced in the fitting procedures, we propose an alternative method that uses MRM to obtain the $N_0 - W$ relation. In MRM, we first seek to establish a relation between two DSD moments. With this relation, the exponential distribution is reduced to having a single free parameter so that N_0 can be determined from W . Suppose that two DSD moments M_l , and M_m are related by a power-law relation:

$$M_l = aM_m^b, \quad (5)$$

where a and b are coefficients that can be estimated from disdrometer observations.

From Eq. (2) for the third moment, we have water content $W = \frac{\pi}{6} \rho M_3 = \pi \rho N_0 \Lambda^4$, [ρ is water density], yielding the slope parameter $\Lambda = \left(\frac{N_0 \pi \rho}{W} \right)^{1/4}$. Substituting (2) into (5) for M_l and M_m , and making use of the relation for Λ , we obtain

$$N_0 = \alpha W^\beta, \quad (6)$$

where

$$\alpha = \left(a \frac{\Gamma^b(m+1)}{\Gamma(l+1) \pi^c \rho^c} \right)^{\frac{1}{1-b+c}}, \quad (7)$$

$$\beta = \frac{c}{1-b+c}, \quad (8)$$

and

$$c = \frac{b(m+1) - (l+1)}{4}. \quad (9)$$

Hence, (6) - (9) constitute a general formulation for deriving a $N_0 - W$ relation using a statistical relation between two DSD moments. When the coefficients a and b in the relation (5) are determined from a set of DSD data, we have a diagnostic relation between the water content W and the intercept parameter N_0 . This is the procedure that will be used in the next section with a disdrometer dataset.

3. Derivation of the $N_0 - W$ relation from disdrometer observations

We test our method for deriving the $N_0 - W$ relation using disdrometer data collected in Oklahoma during the summer seasons of 2005, 2006 and 2007 (Cao et al. 2008). Three 2DVDs, operated respectively by the University of Oklahoma (OU), National Center for Atmospheric

Research (NCAR) and National Severe Storms Laboratory (NSSL) were deployed at the NSSL site in Norman, Oklahoma, and at the Southern Great Plains (SGP) site of the Atmospheric Radiation Measurement (ARM) program. The ARM site is located approximately 28 km south of the NSSL site. The three 2DVDs have similar characteristics, but with slightly different resolutions. The OU and NCAR disdrometers have the same resolution of 0.132 mm while the NSSL disdrometer has a 0.195 mm resolution. The resolutions limit the performance and accuracy in measuring very small drops ($D < 0.4$ mm). A total of 14200 minutes of disdrometer data with total drop counts greater than 50 were collected. The recorded raindrops within each minute were processed to produce one-minute DSD samples, resulting in 14200 DSDs. Among them, only 870 DSDs are side-by-side measurements, yielding 435 pairs of DSDs.

With the side-by-side data, measurement errors of DSDs were quantified. The sampling errors are further reduced by sorting and averaging based on two parameters (SATP), a method that combines DSDs with similar rainfall rates (R) and median volume diameters (D_0) (Cao et al. 2008). There are 2160 quality-controlled DSDs after SATP processing for the same dataset (14200 DSDs). The DSD moments are estimated by the sum of weighted DSDs as defined in (2). As shown in Table 1 of Cao et al. (2008), the relative errors of the moments: M_0 , M_2 , M_3 , M_4 and M_6 are: 10.3, 9.1, 9.0, 10.3, and 17.5%, respectively. In addition, the low moment measurements are highly affected by wind, splashing and instrumentation limits, resulting in even more error that is not shown in that table (Kruger and Krajewski 2002). Since the middle moments (M_2 , M_3 , M_4) are measured more accurately, their use in DSD fitting should be more reliable. It is desirable to consider both error effects and physical significance of the moments being used for the application. A moment pair (M_2 , M_4) is considered a good combination that balances both well

(Smith and Kliche, 2005). In addition, the moment pair (M_2, M_4) has an advantage over (M_2, M_3) or (M_3, M_4) because of the larger difference in the information the two moments provide.

As an example, three measured rain DSDs are shown in Fig. 1 as discrete points. Based on rain rate and precipitation duration, they correspond to strong convection (A: 2231 UTC), weak convection (B: 2344 UTC) and stratiform rain (C: 2301 UTC), respectively, taken from the rain events shown in Figs. 5c and 6c. Using the moment pair of (M_2, M_4) , the DSDs are fitted to the exponential distribution, shown as dashed lines. The exponential DSD model fits the data reasonably well, especially for the strong convection and stratiform rain cases. It is also noted that the exponential model does not capture well the curved shape of stratiform and weak convection DSDs (see, e.g., Fig. 3 of Brandes et al. 2006). In those instances, it tends to overestimate the number concentration. It is clear that the intercept parameter values are quite different for strong convection, weak convection and stratiform DSDs; however, there seems to be a systematic/statistical trend: the heavier the rain intensity, the larger the N_0 value.

In the DFA, the exponential DSD parameters N_0 and Λ are first estimated from the moment pairs of (M_0, M_3) , (M_2, M_4) , and (M_3, M_6) using Eqs. (3) and (4) for the whole dataset. The exponentially-fitted N_0 values are plotted versus the rain water content in Fig. 2. The rain water content is calculated from the estimated 3rd moment by $W = \frac{\pi}{6} \times 10^{-3} M_3$ from measured DSDs.

As expected, there is a large scatter in the $N_0 - W$ plot because of measurement and model errors as well as natural variations. It is important to note that the N_0 variability is part of rain microphysical properties, represented by the exponential DSD model. Also, different moment pairs produce different results for N_0 due to differences in estimation error and error propagation in the fitting procedure (Zhang et al. 2003). It is clear that there is a positive correlation between N_0 and W .

However, due to the large scatter of data points in Fig. 2, it is difficult to fit them to stable $N_0 - W$

relations. For example, minimizing error in the x-axis (W) gives a different result from that of minimizing error in the y-axis (N_0). We chose to minimize the errors on both axes, yielding the results shown in Fig. 2 as straight lines. The coefficients (α , β) for these power-law relations are listed in Table 1. As discussed earlier, the most reliable result is that from the pair (M_2 , M_4), which is

$$N_0^{(D)}(M_2, M_4) = 24144W^{1.326}. \quad (10)$$

Even after minimizing errors on both axes, the results are not optimized, due to the large scatter of the data.

In the MRM, however, an $N_0 - W$ relation is derived from a moment relation as outlined in section 2. Figure 3 shows the scatter plots of moments for the pair of (M_0 , M_3), (M_2 , M_4) and (M_3 , M_6) directly calculated from the DSD data, and the corresponding power-law relations are obtained as

$$M_0 = 0.962M_3^{1.040}, \quad (11a)$$

$$M_2 = 1.473M_4^{0.838}, \quad (11b)$$

$$M_3 = 3.038M_6^{0.626}. \quad (11c)$$

For the moment pair (M_2 , M_4), we have $a = 1.473$ and $b = 0.838$ in Eq. (5). The correlation between the moments is high, with a correlation coefficient of 0.85 in the linear domain and 0.90 in the logarithmic domain for this pair. Substituting for a and b in (6)-(9), we obtain $\alpha = 7106$ and $\beta = 0.648$, therefore

$$N_0^{(M)}(M_2, M_4) = 7106W^{0.648}. \quad (12)$$

The results with the other moment pairs of (M_0 , M_3) and (M_3 , M_6) are shown in Table 1 with their coefficients. This $N_0 - W$ relation (12) derived from the moment pair (M_2 , M_4) is shown in Fig. 4 along with those derived from moment pairs (M_0 , M_3) and (M_3 , M_6) as thick lines. The

lower (higher) moment pair yields a relation with a larger (smaller) slope, which is opposite to the DFA results. Overall, the DFA results have even larger slopes, attributed to the effects of limited number of drops for light rain, since each data point is equally weighted and there are more points for light rain. Nevertheless, they all have an increasing trend with W . The diagnostic relation by Thompson et al. (2004) is also shown for comparison, which has a trend opposite to those indicated by Eqs. (10) and (12), developed here based on disdrometer data. Because the total number concentration is given by $N_t = N_0/\Lambda$ and the median volume diameter is given by $D_0 = 3.67/\Lambda$, the Thompson scheme yields a large (small) total number concentration for light (heavy) rain, which is not true in observations of summer rain events (Zhang et al. 2001). Hence, Thompson's relation proposed for winter weather drizzle may not be suitable for simulating convective and stratiform rain events.

While it is true that the performance of both the DFA and MRM depends on the accuracy of moment estimates, the error propagations in the two approaches are different: Normally, DSD parameters are difficult to estimate with high accuracy from a measured DSD (as in the DFA), especially for light rain with few drops. In MRM, however, a mean moment relation is derived, which may not be affected by the light rain error as much as in the methods used in DFA. As discussed earlier, the middle moment pair (M_2, M_4) has smaller errors and its derived relations should be used. The two $N_0 - W$ relations in (10) and (12), derived using the DFA and MRM methods, and the fixed N_0 are compared through their error statistics. The absolute value of the mass-weighted relative error of moment estimates using the constrained exponential DSD models is calculated as

$$\gamma_n = \frac{\sum_{l=1}^L |M_n^{(e)}(l) - M_n^{(m)}(l)| \times M_3^{(m)}(l)}{\sum_{l=1}^L M_n^{(m)}(l) \times M_3^{(m)}(l)}, \quad (13)$$

where the measured n^{th} moment is $M_n^{(m)}(l)$, which is directly calculated from the l^{th} DSD, $M_n^{(e)}(l)$ is the estimated moment from water content using the diagnostic N_0 DSD model. The results are listed in Table 2. It is shown that the DFA relation (10) yield larger errors, with negative biases for the higher moments (M_4 , M_5 , and M_6), and positive biases for the lower moments (M_0 , M_1 , and M_2). This is because the DFA treats each data point with equal weight in the log-log plot (Fig. 2). The large number of light rain DSDs may dominate the fitted relation, leading to an unrealistically large power coefficient and yielding over- (under-) estimation of N_0 for heavy (light) rain, and hence the negative and positive biases. However, the moment errors with relation (12) are much smaller, especially for the lower moments, because the MRM-derived relation accounts for proper weighting. It is interesting to note that the fixed $N_0 = 8000 \text{ m}^{-3} \text{ mm}^{-1}$ used by the M-P model performs better than the DFA-derived relation. On the other hand, other fixed N_0 values may not yield the same performance. This shows the importance of the procedure used in deriving a diagnostic relation. It is obvious that the MRM relation (12) has the best performance in characterizing rain microphysics. Therefore relation (12) is recommended.

For a better understanding of the $N_0 - W$ relation (12), Figure 5 shows an example of N_0 values along with other physical parameters (N_t , W , and D_0) as a function of time for a convective rain event starting on July 21, 2006. This event was characterized by a strong convective storm followed by weak convection passing over the OU disdrometer deployed at the ARM site in Washington, Oklahoma. The water content is very low during the weak convection periods, but the median volume diameter D_0 is comparable to that during the strong convection. The

comparison between exponentially-fitted N_0 values from DSD moments M_2 and M_4 and those diagnosed from W using (12) is plotted in Fig. 5a. Had the Thompson et al. (2004) relation been plotted, it would have been out of the range of the graph except for the strong convection period. As shown in Fig. 5b, moment fitting of the exponential DSD model yields a good estimate of total number concentration N_t as compared with direct estimates from DSD data (discrete “+”). Here, the fitted N_0 can be considered as “truth” because N_0 is a model parameter which is obtained through the fitting procedure of Eqs. (2) - (4). It is clear that the diagnosed N_0 captures the main trend of the observed rainstorm very well in a dynamic range of more than two orders of magnitude; that is, from an order of 10^4 for strong convection to 10 for light rain precipitation. In comparison, the fixed- N_0 model overestimates N_0 except for heavy convective rain. Figure 5c shows the rain water content directly estimated from the DSD data. Also indicated in the figure are times when the two convection DSDs shown in Fig. 1 are taken. Figure 5d compares median volume diameter D_0 calculated from the DSD data, estimated using the diagnostic- N_0 DSD model and that with the fixed- N_0 DSD model. The diagnostic- N_0 model yields D_0 results arguably better than those of fixed- N_0 model.

Figure 6 shows the same parameters as that in Fig. 5, but for a primarily stratiform rain event that began with weak convection (at 2115 UTC) on November 6, 2006. Again, the diagnostic $N_0 - W$ relation produces a much better agreement with the measurements than does the fixed- N_0 model, especially for D_0 during the stratiform rain period (after 2230 UTC). It is also noted that the stratiform rain has a much lower number concentration ($N_t < 500$) than the strong convection in Fig. 5. Even the exponential fit and the diagnostic N_0 model overestimate N_t by three to four times. This is because stratiform rain DSDs tend to have a convex shape and do not contain as many small drops as the exponential model. Also, since the dataset is dominated by convective rain

events, the derived relation (12) may not represent stratiform rain as well as convective rain. Further reduction of N_0 may be needed for better representing stratiform rain characteristics.

4. Application to warm rain microphysical parameterization

The warm rain microphysical processes related to the DSD include rain evaporation, accretion of cloud water by rain water, and rain sedimentation. Microphysical parameterizations of these processes based on the exponential DSD model have been derived by Kessler (1969: Table 4). After unit conversion, the evaporation rate (R_e in $\text{kg kg}^{-1} \text{ s}^{-1}$), accretion rate (R_c in $\text{kg kg}^{-1} \text{ s}^{-1}$), mass-weighted terminal velocity (V_{tm} in m s^{-1}), and reflectivity factor (Z in $\text{mm}^6 \text{ m}^{-3}$) are given by

$$R_e = 2.17 \times 10^{-5} E_e N_0^{7/20} (q_{vs} - q_v) W^{13/20}, \quad (14a)$$

$$R_c = 1.65 \times 10^{-3} E_c N_0^{1/8} q_c W^{7/8}, \quad (14b)$$

$$V_{tm} = 16.4 N_0^{-1/8} W^{1/8} (\rho_0 / \rho)^{0.5}, \quad (14c)$$

$$Z = 1.73 \times 10^7 N_0^{-3/4} W^{7/4}. \quad (14d)$$

where E_e and E_c are the evaporation and accretion efficiency factors, respectively (normally taken as 1); W is rain water content in g m^{-3} as before ($W = 1000 \rho q_r$); q_v , q_c and q_r are, respectively, the water vapor, cloud water and rain water mixing ratios in kg kg^{-1} .

Substituting the diagnostic relation (12) into (14) and assuming unit saturation deficit and unit cloud water mixing ratio as well as unit efficiency factors, we obtain a parameterization scheme based on the diagnostic- N_0 DSD model. The terms corresponding to those in Eq. (14) are listed in Table 3 along with those of the standard fixed- N_0 M-P model. The coefficients of these terms are similar for the two schemes, but the powers are substantially different. The larger power in evaporation rate means more (less) evaporation for heavy (light) rain compared to the fixed- N_0 model. The smaller power in the reflectivity formula for the diagnostic- N_0 model gives smaller

(larger) reflectivity than the fixed N_0 for heavy (light) rain. This may lead to a better agreement between numerical model forecasts and radar observations. The fixed- N_0 DSD model tends to over-predict large reflectivity values and under-predict low reflectivity values (Brandes et al. 2006). In this sense, the diagnostic- N_0 model has similar properties as the simplified constrained Gamma model investigated in Zhang et al. (2006).

Figure 7 compares the two parameterization schemes based on the diagnostic- N_0 and fixed- N_0 DSD models, respectively, by showing the microphysical processes/parameters as a function of W . The direct calculations from the DSD dataset are also shown for comparison. The diagnostic- N_0 results agree well with that from the measurements except for reflectivity. The mass-weighted error of the reflectivity estimates with the diagnostic N_0 , however, is smaller than that of the fixed N_0 , as indicated in Table 2. As stated in the previous paragraph, the diagnostic- N_0 model yields smaller (larger) evaporation and accretion rates for light (heavy) rain than the fixed- N_0 model. However, the diagnostic- N_0 scheme gives large (small) reflectivity and mass-weighted velocity values for light (heavy) rain cases. It is noted that the low end of the data points in Fig. 7b are associated with light rain and have large sampling errors. The performance of the DSD models should also be evaluated by calculating the relative errors for all the moments, as given in Table 2 and discussed earlier.

Figure 8 and 9 compare the terms for the microphysical processes estimated from W with the diagnostic- N_0 scheme with those from the fixed- N_0 scheme for the two rain events shown in Figs. 5 and 6. Direct calculations from the observed DSD data and those with the exponential scheme with N_0 as one of the two free parameters are also shown for reference. The results may appear to be close to each other in the semi-logarithm plots but actually, the fixed- N_0 scheme underestimates evaporation rate for strong convection (2220–2240 UTC) as the dashed line is

below the red line and has smaller values than that of the direct calculations in Fig. 8. However, the scheme overestimates the evaporation rate for stratiform rain by about a factor of five, shown in Fig. 9. This might be the reason that the parameterization coefficients in the Kessler scheme are sometimes reduced by a half or more in order to obtain a better match of modeling results with observations (e.g., Miller and Pearce 1974; Sun and Crook 1997). The diagnostic- N_0 scheme also performs slightly better than the fixed- N_0 scheme in estimating accretion rate and mass-weighted terminal velocity, which is visible in Figs. 7, 8 and 9 except for a few missing points. Therefore the diagnostic- N_0 scheme characterizes rain evaporation, accretion and rainfall processes more accurately than the fixed- N_0 model for both heavy and light rainfall. By introducing the dependency of N_0 on W based on observations, raindrop number concentration and total surface area of rain drops are better represented, leading to a better estimation of evaporation and accretion rates.

5. Summary and Discussions

In this paper, we present a method for diagnosing the intercept parameter N_0 of the exponential drop size distribution (DSD) based on water content W , and apply the diagnostic- N_0 DSD model towards improving warm rain microphysical parameterization. The diagnostic relation is derived from a relation between two DSD moments that are estimated from 2D video disdrometer data. The DSD data were collected in Oklahoma during the summer seasons of 2005 and 2006, which should be representative for rain events in the central Great Plains region. The diagnostic $N_0 - W$ relation is used to improve the Kessler parameterization scheme of warm rain microphysics, and can be used in schemes containing ice phases also (e.g., those in commonly used schemes of Lin et al. 1983 and Hong et al. 2004).

It has been shown that the diagnostic- N_0 model better characterizes natural rain DSDs, including the physical properties (e.g., N_t and D_0) and microphysical processes. For a given water content, the diagnostic- N_0 DSD model represents the total number concentration, median volume diameter, reflectivity factor, evaporation rate and accretion rate more accurately than the M – P model with a fixed N_0 . Compared with the M-P model-based Kessler scheme, the modified parameterization scheme with a diagnostic N_0 has the following advantages: (i) it leads to less (more) evaporation for light (heavy) rain and therefore can preserve stratiform rain better in numerical models, and (ii) it yields a larger (smaller) reflectivity factor for light (heavy) rain, having the potential of yielding a better agreement between model-predicted and radar-observed reflectivities in a way similar to the simplified constrained Gamma model. Realistic simulation of reflectivity is important for assimilating radar reflectivity data into NWP models.

It is noted that the diagnostic $N_0 - W$ relation obtained in this paper is based on a specific set of disdrometer data in a specific climate region, dominated by convective rain events. While the methodology developed in this paper is general, the coefficients in the relation may require tuning in order for them to better fit specific regions and/or seasons or specific rain types. For example, the coefficient of (12) may need to be reduced by a factor of two to three to better represent stratiform rain characteristics. The improved parameterization based on the diagnostic- N_0 model is now being tested within a mesoscale model for real events to examine its impact on precipitation forecasts; the results will be presented in the future.

Acknowledgments. Authors greatly appreciate the help of data collection from Drs. Edward Brandes, Terry Schuur, Robert Palmer, Phillip Chilson and Ms. Kyoko Iketa. The sites for disdrometer deployment at the Kessler farm were provided by Atmospheric Radiation

Measurement (ARM) Program. This work was primarily supported by NSF grant ATM-0608168. Ming Xue and Dan Dawson were also supported by NSF grants ATM-0530814, ATM-0331594 and ATM-0331756.

References

- Brandes, E. A., G. Zhang, and J. Vivekanandan, 2002: Experiments in rainfall estimation with a polarimetric radar in a subtropical environment. *J. Appl. Meteor.*, **41**, 674-685.
- Brandes, E. A., G. Zhang, and J. Sun, 2006: On the influence of assumed drop size distribution form on radar-retrieved thunderstorm microphysics. *J. Appl. Meteor. Climat.*, **45**, 259-268,
- Cao, Q., G. Zhang, E. Brandes, T. Schuur, A. Ryzhkov, and K. Ikeda, 2008: Analysis of video disdrometer and polarimetric radar data to characterize rain microphysics in Oklahoma. To appear in *J. Appl. Meteor. Climat.*
- Gilmore, M. S., J. M. Straka, and E. N. Rasmussen, 2004: Precipitation uncertainty due to variations in precipitation particle parameters within a simple microphysics scheme. *Mon. Wea. Rev.*, **132**, 2610-2627.
- Hong, S.-Y., J. Dudhia, and S.-H. Chen, 2004: A revised approach to ice microphysical processes for the bulk parameterization of clouds and precipitation. *Mon. Wea. Rev.*, **132**, 103–120.
- Kessler, E., 1969: On the distribution and continuity of water substance in atmospheric circulations. *Meteor. Monogr.*, No. 32, Amer. Meteor. Soc., 84 pp.
- Kruger, A. and W. F. Krajewski, 2002: Two-Dimensional Video Disdrometer: A Description, *J. Atmos. Ocean. Tech.*, **19**, 602-617.
- Lin, Y.-L., R. D. Farley, and H. D. Orville, 1983: Bulk parameterization of the snow field in a cloud model. *J. Climate Appl. Meteor.*, **22**, 1065–1092.
- Marshall, J.S., and W. McK. Palmer, 1948: The distribution of raindrops with size, *J. Meteor.*, **5**, 165-166.
- Meyers, M. P., R. L. Walko, J. R. Harrington, and W. R. Cotton, 1997: New RAMS cloud

- microphysics parameterization. Part II: The two-moment scheme. *Atmos. Res.*, **45**, 3-39.
- Milbrandt, J. A. and M. K. Yau, 2005a: A multi-moment bulk microphysics parameterization. Part I: Analysis of the role of the spectral shape parameter. *J. Atmos. Sci.*, **62**, 3051-3064.
- Milbrandt, J. A. and M. K. Yau, 2005b: A multi-moment bulk microphysics parameterization. Part II: A proposed three-moment closure and scheme description. *J. Atmos. Sci.*, **62**, 3065-3081
- Miller, M. J., and R. P. Pearce, 1974: A three-dimensional primitive equation model of cumulonimbus convection. *Quart. J. Roy. Meteor. Soc.*, 100, 133–154.
- Sauvageot, H., and J.-P. Lacaux, 1995: The shape of averaged drop size distributions. *J. Atmos. Sci.*, **52**, 1070–1083.
- Seifert A, 2005: On the shape-slope relation of drop size distributions in convective rain. *J. Appl. Meteor.*, **44** (7), 1146-1151.
- Smith, P. L., and D. V. Kliche, 2005: The Bias in Moment Estimators for Parameters of Drop Size Distribution Functions: Sampling from Exponential Distributions, *J. Appl. Meteor.*, **44**, 1195–1205.
- Steiner, M., J. A. Smith, and R. Uijlenhoet, 2004: A microphysical interpretation of radar reflectivity-rain rate relationships. *J. Atmos. Sci.*, **61**, 1114-1131.
- Sun, J, and N. A. Crook, 1997: Dynamical and microphysical retrieval from Doppler radar observations using a cloud model and its adjoint. Part I: Model development and simulated data experiments. *J. Atmos. Sci.*, 54, 1642–1661.
- Thompson, G., R. M. Rasmussen, and K. Manning, 2004: Explicit forecasts of winter Precipitation using an improved bulk microphysics scheme. Part I: Description and Sensitivity Analysis, *Mon. Wea. Rev.*, **132**, 519-542
- Tong, M. and M. Xue, 2008: Simultaneous estimation of microphysical parameters and

- atmospheric state with radar data and ensemble square-root Kalman filter. Part I: Sensitivity analysis and parameter identifiability *Mon. Wea. Rev.*, In press.
- Van den Heever, S.C., and W.R. Cotton, 2004: The impact of hail size on simulated supercell storms, *J. Atmos. Sci.*, **61**, 1596-1609.
- Waldvogel, A., 2006: The N_0 Jump of raindrop Spectra. *J. Atmos. Sci.*, **31**, 1067-1078.
- Walko, R.L., W.R. Cotton, M.P. Meyers and J.Y. Harrington, 1995: New RAMS cloud microphysics parameterization. Part I: The single-moment scheme, *Atmos. Res.*, **38**, 29-62.
- Zhang, G., J. Vivekanandan, and E. Brandes, 2001: A method for estimating rain rate and drop size distribution from polarimetric radar measurements. *IEEE Trans. Geosci. Remote Sens.*, **39**, 830–841.
- Zhang, G., J. Vivekanandan, E.A. Brandes, R. Meneghini, and T. Kozu, 2003: The shape-slope relation in Gamma raindrop size distribution: statistical error or useful information?, *J. Atmos. Ocean. Tech.*, **20**. 1106-1119.
- Zhang, G., J. Sun, and E. A. Brandes, 2006: Improving parameterization of rain microphysics with disdrometer and radar observations. *J. Atmos. Sci.*, **63**, 1273-1290.

Figure captions

Fig. 1: Examples of raindrop size distributions and their fit to the exponential distribution using the moment pair (M_2, M_4) . The four DSDs correspond to strong convection, weak convection and stratiform rain.

Fig. 2: Dependence of intercept parameter (N_0) on water content (W) . Scattered points are fitted results from a pair of DSD moments. Straight lines are derived relations using the direct fitting method.

Fig. 3: Inter-relationships among DSD moments based on disdrometer measurements. Scattered points are direct estimates from disdrometer measurements. Straight lines represent fitted power-law relations. (a): M0-M3, (b): M2-M4, and (c): M3:M6.

Fig. 4: Results of diagnostic N_0 - W relations using the moment relation method. The results of the direct fitting approach and the Thompson et al. (2004) approach are shown for comparison.

Fig. 5: Time series comparison of physical parameters: intercept parameter (N_0) , total number concentration (N_t) water content (W) , and median volume diameter (D_0) for a convective rain event starting on July 21, 2006. Results are shown for disdrometer measurements and fitted values using exponential, diagnostic- N_0 , and fixed- N_0 DSD models. “A” and “B” correspond to strong and weak convection, respectively. Their DSDs are shown in Fig.1.

Fig. 6: As in Fig. 5 but for a stratiform rain event on November 6, 2006. “C” is identified as stratiform rain whose DSD is shown in Fig. 1.

Fig. 7: Comparison of rain physical process parameters for a unit saturation deficit and cloud water mixing ratio between the diagnostic N_0 and fixed DSD models. (a) R_e and R_c in $\text{kg kg}^{-1} \text{s}^{-1}$, and V_{tm} in m s^{-1} , and (b) reflectivity Z in $\text{mm}^6 \text{m}^{-3}$

Fig. 8: As in Fig. 5 except for evaporation rate for a unit vapor saturation deficit (R_e), accretion rate (R_c) for a unit cloud water content, and mass-weighted terminal velocity (V_{tm})

Fig. 9: As in Fig. 8 for the stratiform rain event on November 6, 2006

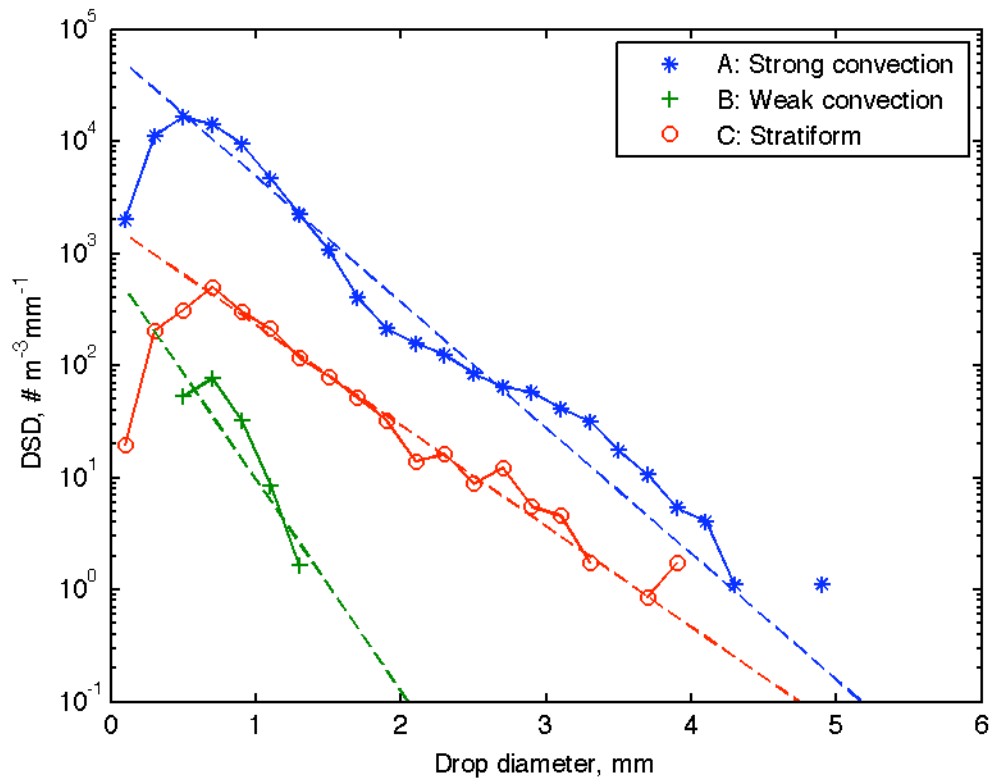


Fig. 1: Examples of raindrop size distribution and their fits to exponential distribution using the moment pair (M_2, M_4) , The three DSDs correspond to strong convection, weak convection and stratiform rain.

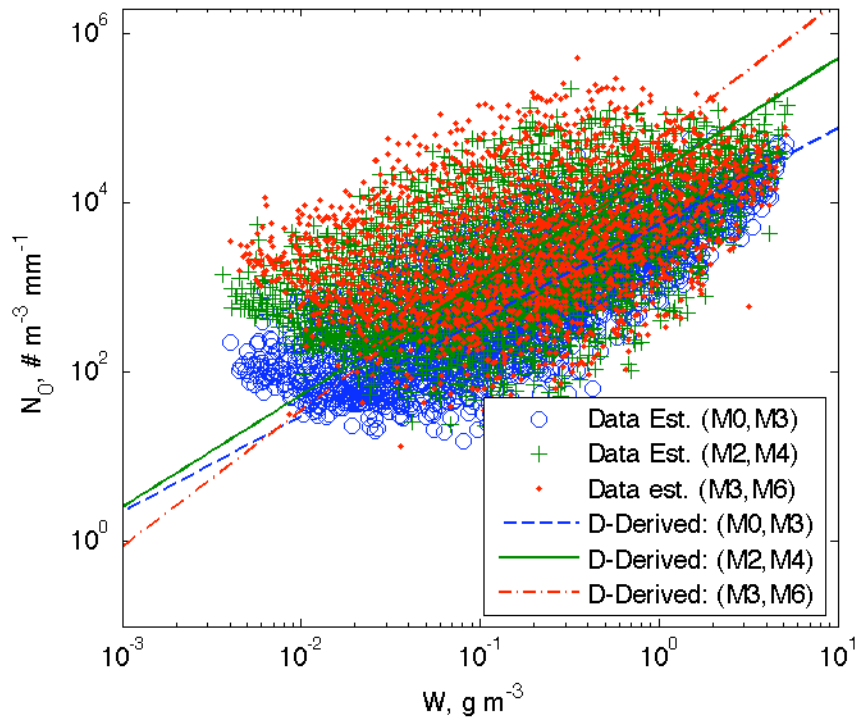


Fig. 2: Dependence of intercept parameter (N_0) on water content (W). Scattered points are fitted results from a pair of DSD moments. Straight lines are derived relations using the direct fitting method.

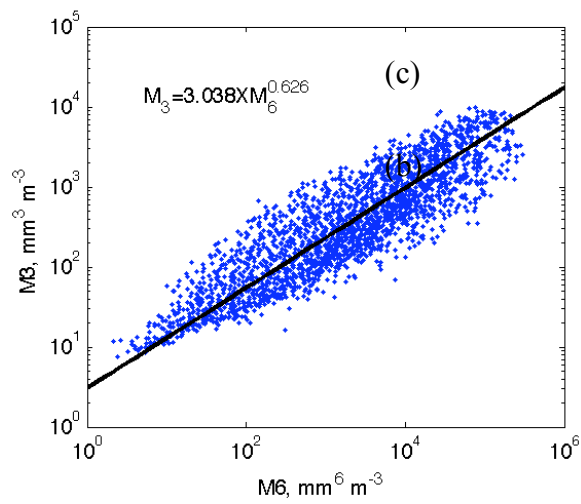
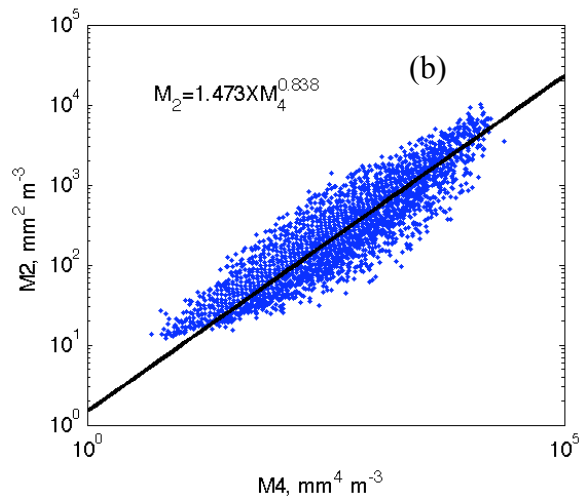
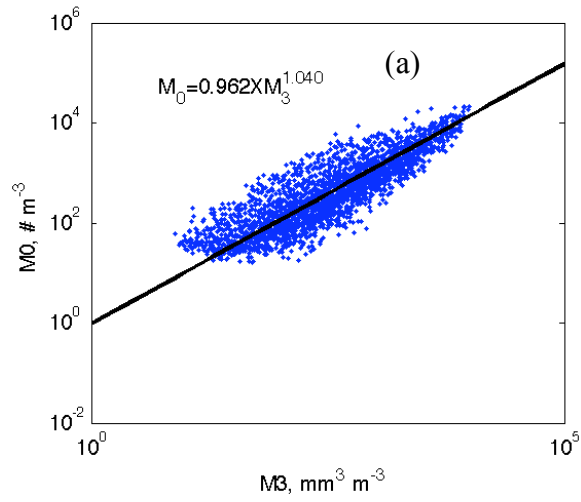


Fig. 3: Inter-relationships among DSD moments based on disdrometer measurements. Scattered points are direct estimates from disdrometer measurements. Straight lines represent fitted power-law relations. (a): M0-M3, (b): M2-M4, and (c): M3:M6.

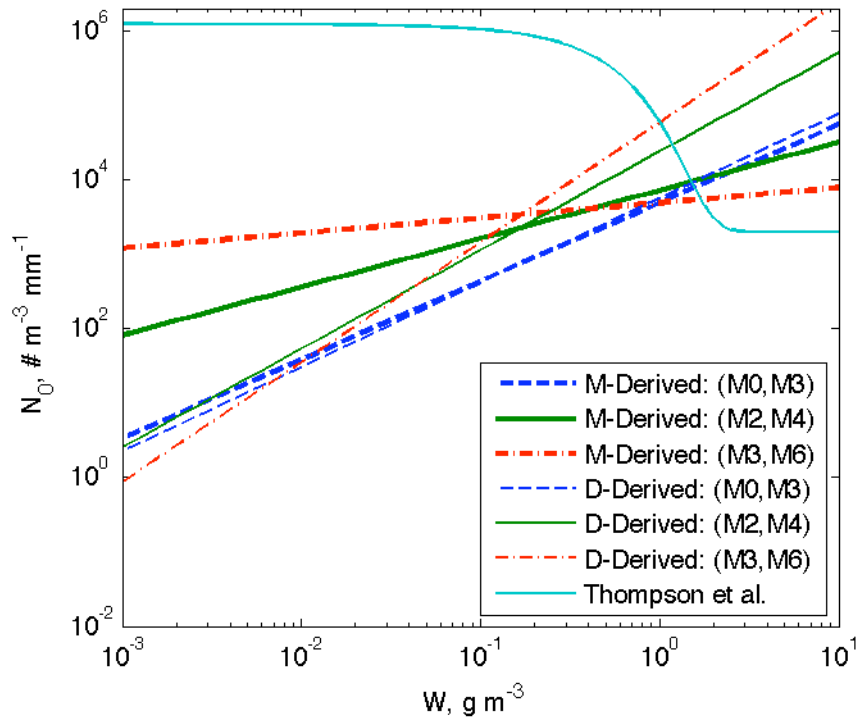


Fig. 4: Diagnostic N_0 - W relations obtained using the moment relation method. The results of the direct fitting approach and the Thompson et al. (2004) approach are shown for comparison.

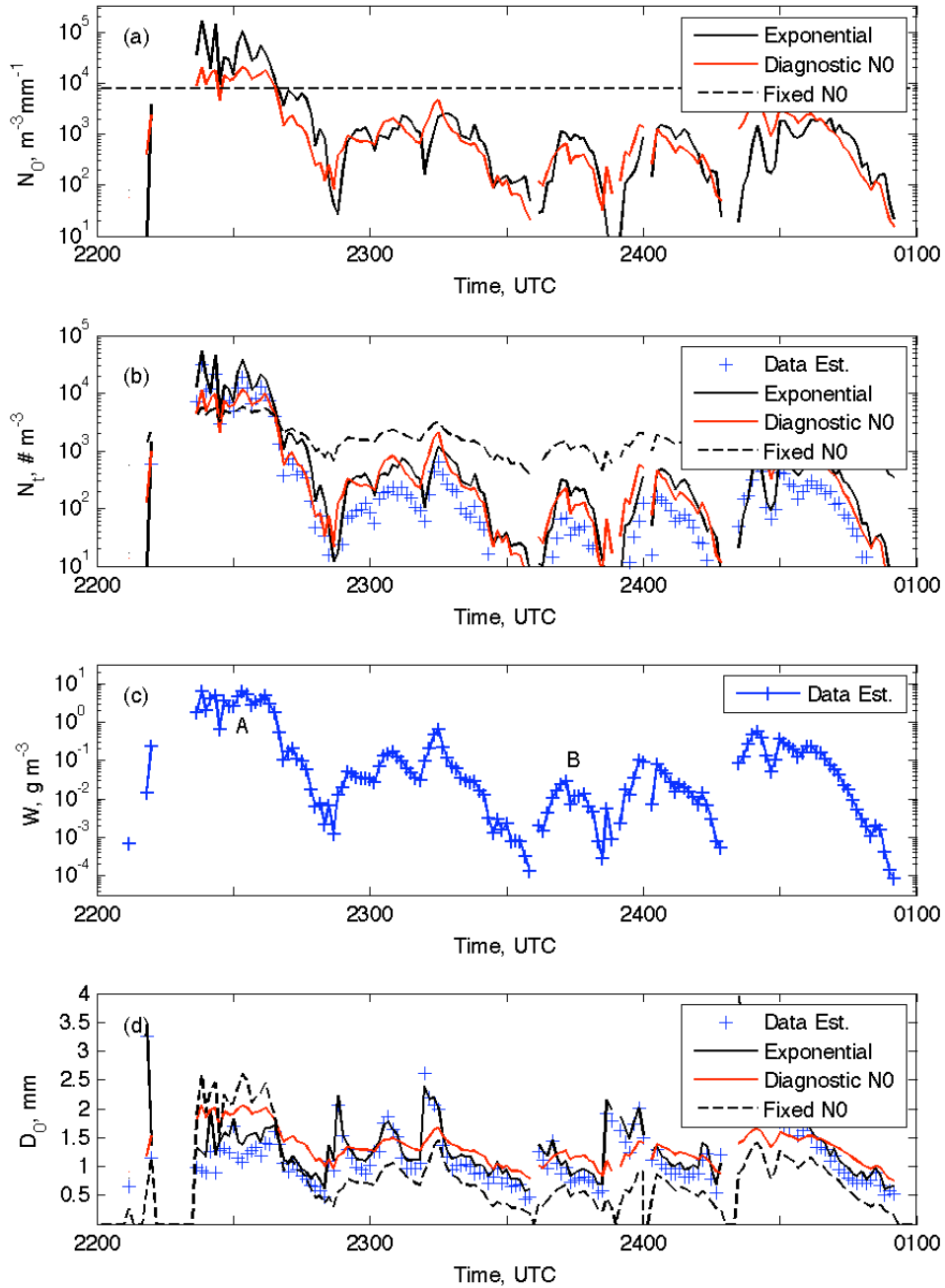


Fig. 5: Time series of intercept parameter (N_0), total number concentration (N_t), water content (W), and median volume diameter (D_0) for a convective rain event starting on July 21, 2006, for disdrometer measurements and fitted values using exponential, diagnostic- N_0 , and fixed- N_0 DSD models. “A” and “B” correspond to strong and weak convection, respectively. Their DSDs are shown in Fig.1.

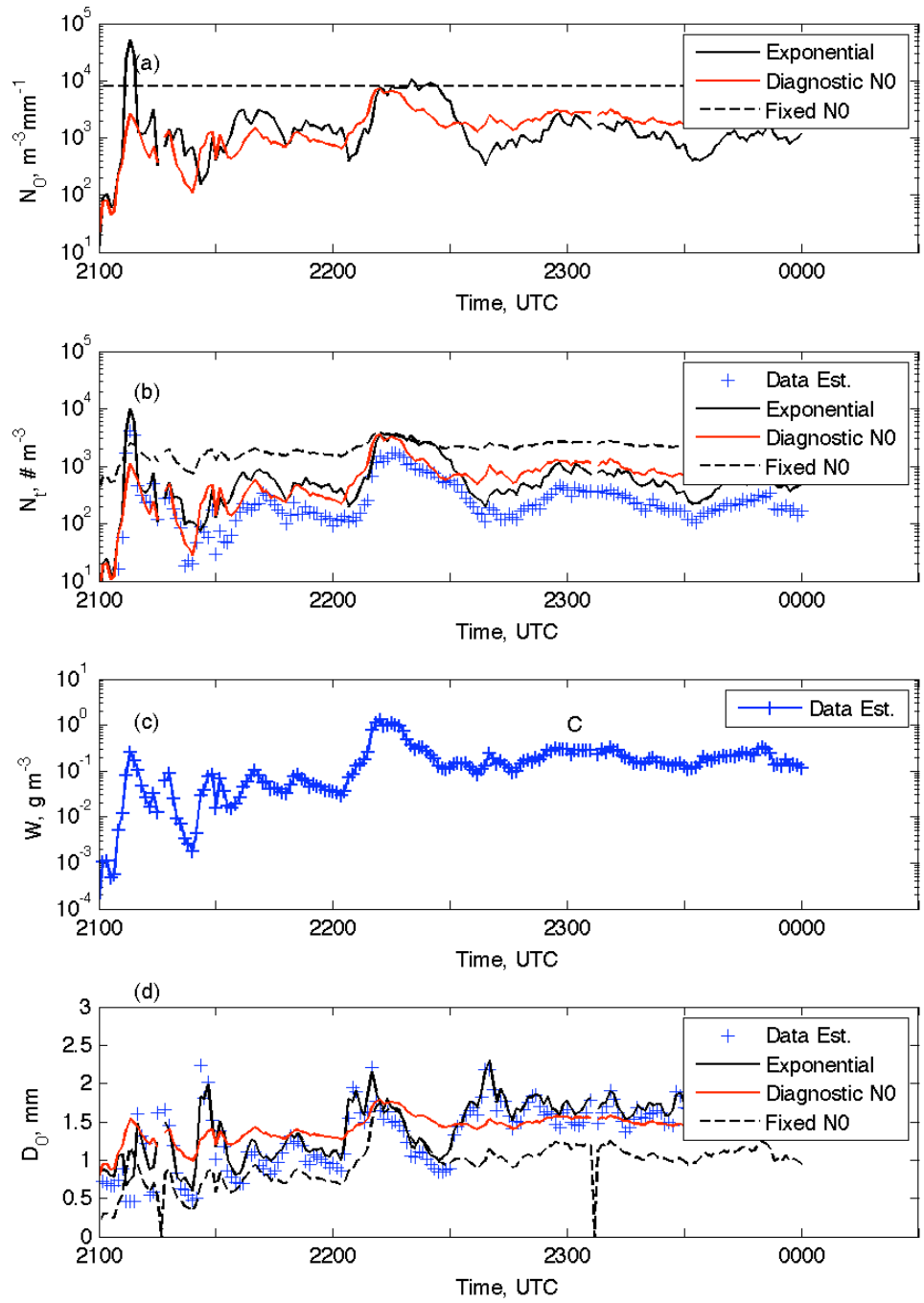


Fig. 6: As Fig. 5 for a stratiform rain event on November 6, 2006. “C” is identified as stratiform rain whose DSD is shown in Fig. 1.

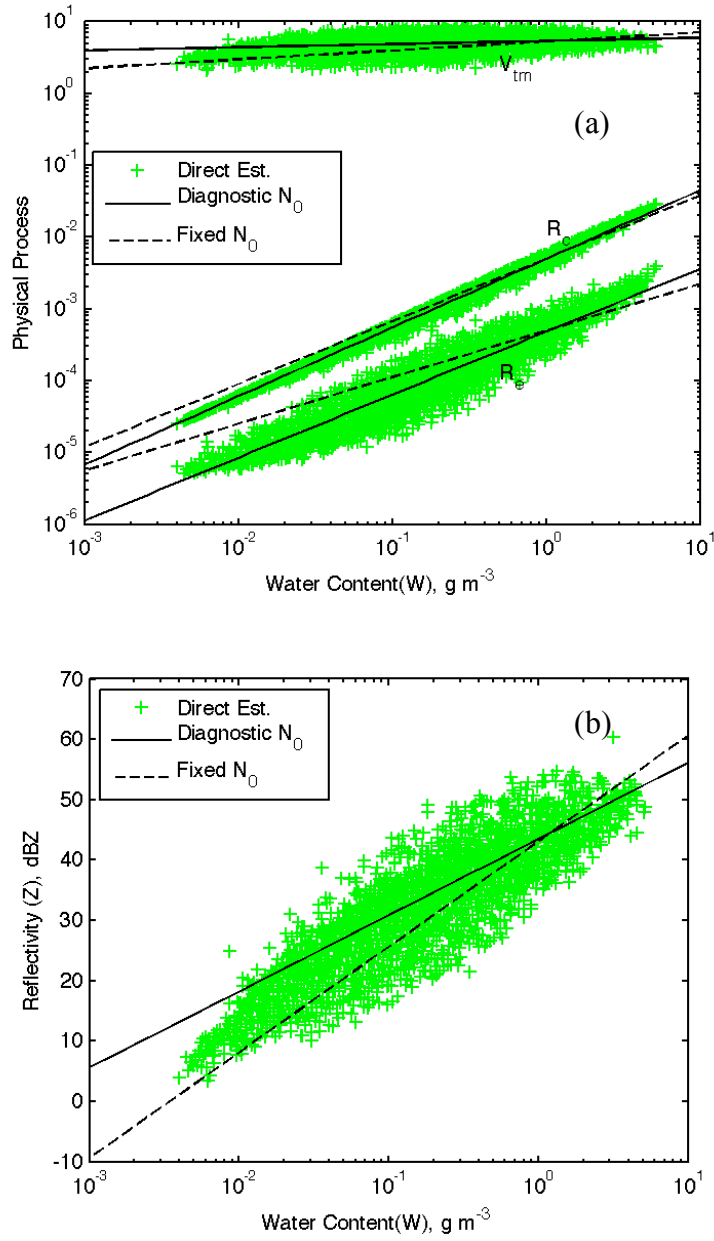


Fig. 7: (a) Rain evaporation rate R_e and accretion rate R_c in $\text{kg kg}^{-1} \text{s}^{-1}$, and terminal velocity V_{tm} in m s^{-1} , and (b) reflectivity Z in $\text{mm}^6 \text{m}^{-3}$, when calculated based on the diagnostic- N_0 and fixed- N_0 DSD models for a unit saturation deficit and unit cloud water mixing ratio.

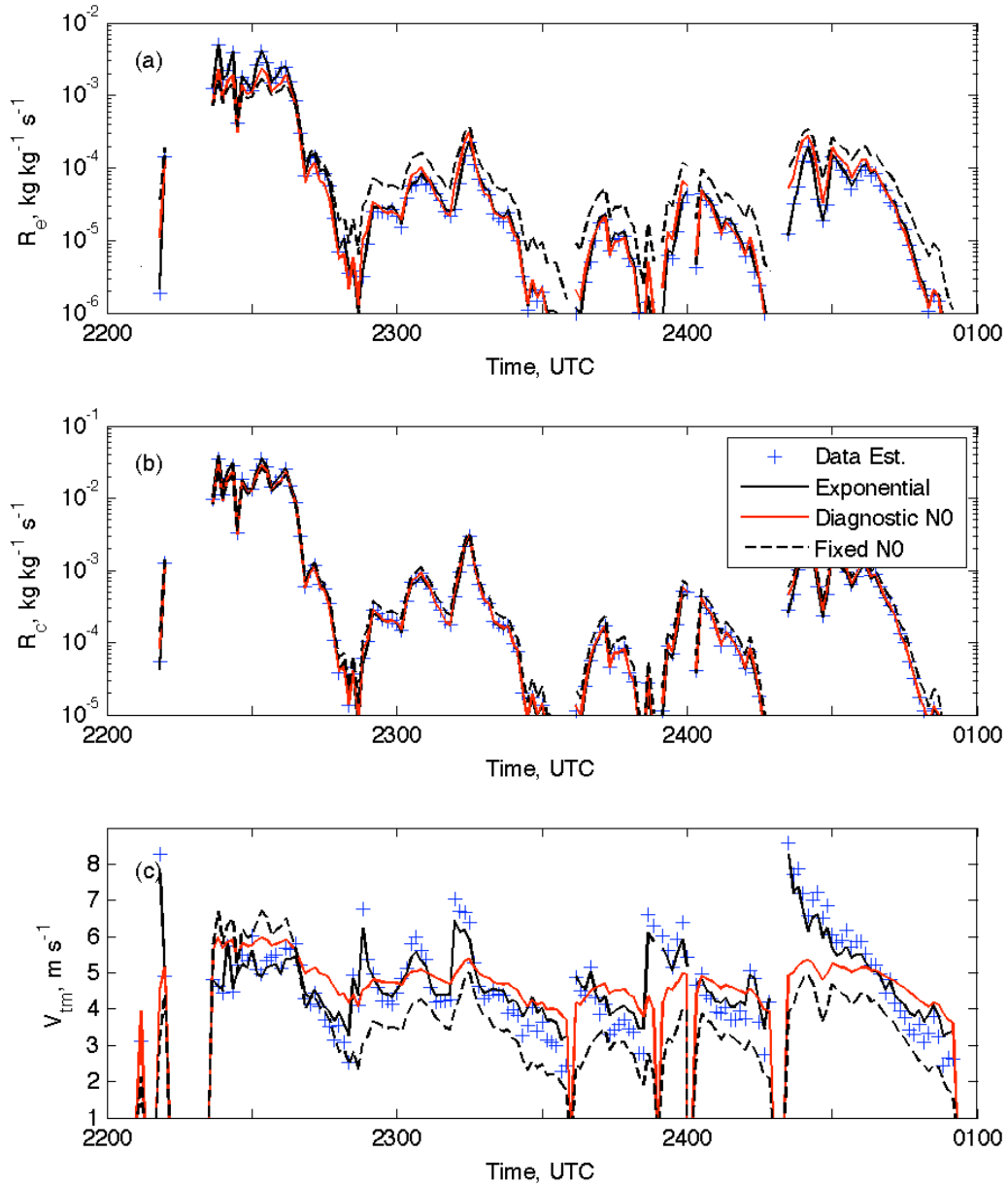


Fig.8: Rain evaporation rate (R_e) for a unit vapor saturation deficit (a), accretion rate (R_c) for a unit cloud water content (b), and mass-weighted terminal velocity (V_{tm}) (c), for a convective rain event starting on July 21, 2006, for disdrometer measurements and fitted values using exponential, diagnostic- N_0 , and fixed- N_0 DSD models.

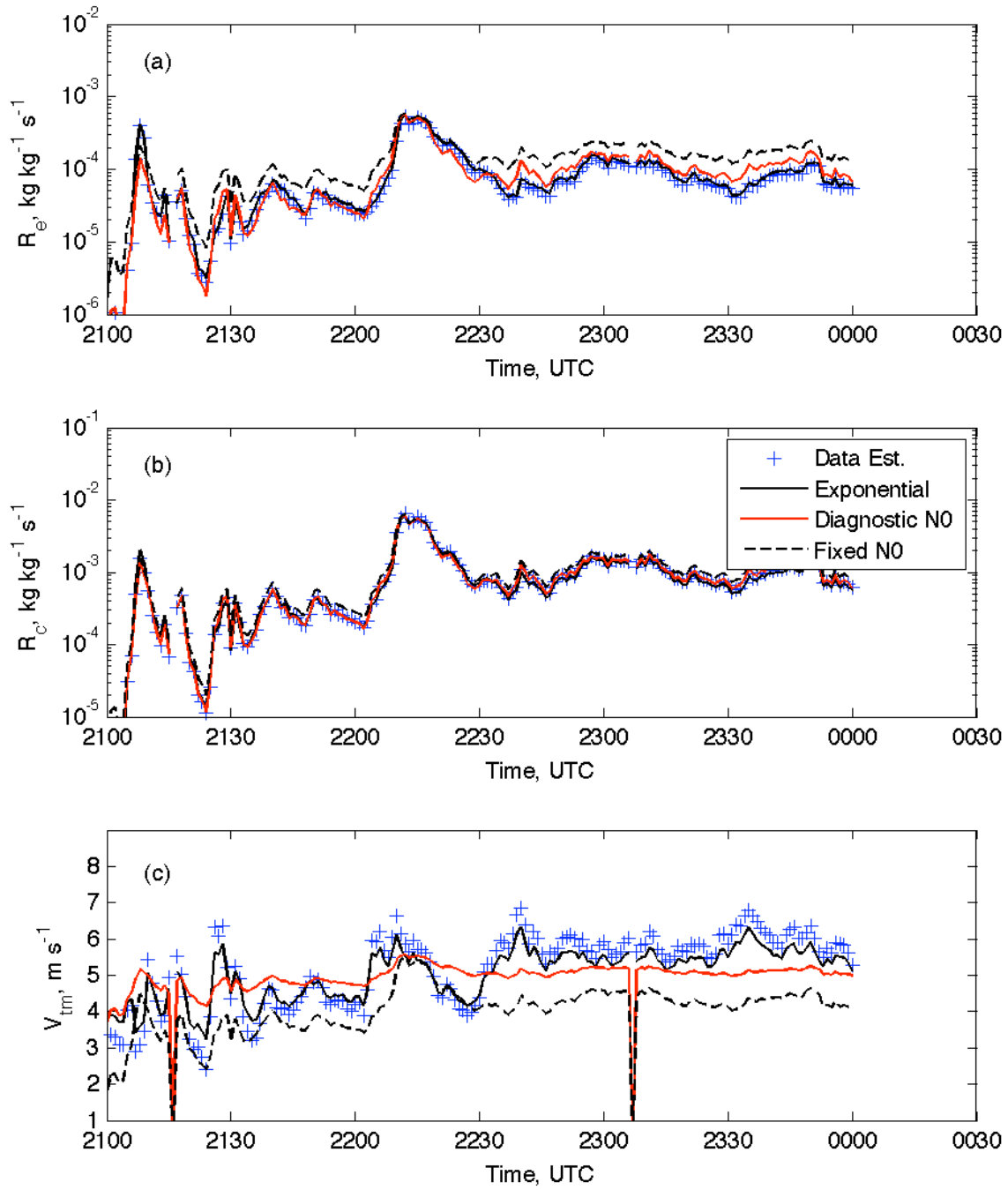


Fig. 9: As Fig. 8 but for the stratiform rain event on November 6, 2006

Table 1: Coefficients of diagnostic N_0 -W relations

Moment pair	DFA		MRM	
	α	β	α	β
M_0, M_3	5674	1.135	4910	1.053
M_2, M_4	24144	1.326	7106	0.648
M_3, M_6	58842	1.611	4903	0.204

Table 2: Comparison of relative errors of moment estimates

Moment		M_0	M_1	M_2	M_3	M_4	M_5	M_6
$\gamma_n, \%$	DFA: Eq. (10)	285.6	90.4	35.1	0.0	32.6	59.8	78.0
	MRM: Eq. (12)	41.9	34.9	21.9	0.0	24.4	45.3	62.5
	M-P: fixed N_0	59.3	47.9	29.6	0.0	35.9	69.5	97.0

Table 3: Parameterization of warm rain processes with diagnostic N_0 and fixed N_0

Parameterized quantity	Diagnostic N_0	Fixed N_0
$N_0, \text{m}^{-3} \text{mm}^{-1}$	$7106W^{0.648}$	8000
$R_e, \text{kg kg}^{-1} \text{s}^{-1}$	$4.84 \times 10^{-4} W^{0.878}$	$5.03 \times 10^{-4} W^{0.65}$
$R_c, \text{kg kg}^{-1} \text{s}^{-1}$	$5.0 \times 10^{-3} W^{0.956}$	$5.08 \times 10^{-3} W^{0.875}$
$V_{\text{tm}}, \text{m s}^{-1}$	$5.41W^{0.044}$	$5.32W^{0.125}$
$Z, \text{mm}^6 \text{m}^{-3}$	$2.24 \times 10^4 W^{1.264}$	$2.04 \times 10^4 W^{1.75}$